Furanoditerpenoid biosynthesis in the bioenergy crop switchgrass is catalyzed by an alternate metabolic pathway

Andrew Muchlinski[1#], Meirong Jia[1#^], Kira Tiedge[1£], Jason S. Fell[2£], Kyle A. Pelot[1], Lisl Chew[1], Danielle Davisson[1], Yuxuan Chen[1], Justin Siegel[2,3,4], John T. Lovell[5], Philipp Zerbe[1*]

[1]Department of Plant Biology, University of California-Davis, Davis, CA, USA.
[2]Genome Center, University of California-Davis, Davis, CA, USA.
[3]Department of Chemistry, University of California-Davis, Davis, CA, USA.
[4]Department of Biochemistry & Molecular Medicine, University of California-Davis, Davis, CA, USA.
[5]Genome Sequencing Center, Hudson Alpha Institute for Biotechnology, Huntsville, AL, USA.

*To whom correspondence should be addressed: Philipp Zerbe; email: pzerbe@ucdavis.edu; phone: (530) 754-9652; ORCID ID: 0000-0001-5163-9523.

[#,£] These authors contributed equally to this work.

[^]Current address: State Key Laboratory of Bioactive Substance and Function of Natural Medicines & NHC Key Laboratory of Biosynthesis of Natural Products, Institute of Materia Medica, Chinese Academy of Medical Sciences & Peking Union Medical College, Beijing 100050, China.

Key words. Cytochrome P450 monooxygenase, diterpenoid biosynthesis, plant specialized metabolism, plant natural products, *Panicum virgatum*.

Abbreviations. diTPS, diterpene synthase; P450, cytochrome P450 monooxygenase; CPS, copalyl diphosphate synthase; KSL, kaurene synthase-like; Pv, *Panicum virgatum*; GGPP, geranylgeranyl pyrophosphate; CPP, copalyl pyrophosphate; LPP, labda-13-en-8-ol pyrophosphate; CLPP, clerodienyl pyrophosphate; GC-MS, gas chromatography-mass spectrometry; HPLC, high-performance liquid chromatography; NMR, nuclear magnetic resonance; IE, interaction energy; REU, Rosetta energy units; SWC, soil water content.

Significance Statement

Diterpenoids play important roles in stress resilience and chemically mediated interactions in many plant species, including major food and bioenergy crops. Enzymes of the cytochrome P450 monooxygenase family catalyze the various functional decorations of core diterpene scaffolds that determine the large diversity of biologically active diterpenoids. This study describes the identification and mechanistic analysis of an unusual group of cytochrome P450 monooxygenases, CYP71Z25-29, from the bioenergy crop switchgrass (*Panicum virgatum*). These enzymes catalyze the furan ring addition directly to class II diterpene synthase products, thus bypassing the conserved pairwise reaction of class II and class I diterpene synthases in labdane diterpenoid metabolism. Insight into the distinct substrate-specificity of CYP71Z25-29 offers opportunity for engineering of furanoditerpenoid bioproducts.

Abstract

Specialized diterpenoid metabolites are important mediators of stress resilience in monocot crops. A deeper understanding of how species-specific diterpenoid-metabolic pathways and functions contribute to plant chemical defenses can enable crop improvement strategies. Here, we report the genomics-enabled discovery of five cytochrome P450 monooxygenases (CYP71Z25-29) that form previously unknown furanoditerpenoids in the monocot bioenergy crop switchgrass (*Panicum virgatum*). Combinatorial pathway reconstruction showed that CYP71Z25-29 catalyze furan ring addition to diterpene alcohol intermediates derived from distinct class II diterpene synthases, thus bypassing the canonical role of class I diterpene synthases in plant diterpenoid metabolism. Transcriptional co-expression patterns and presence of select diterpenoids in droughted switchgrass roots support possible roles of CYP71Z25-29 in abiotic stress responses. Integrating molecular dynamics, structural analysis, and targeted mutagenesis, identified active site determinants controlling distinct CYP71Z25-29 catalytic specificities and, combined with broad substrate promiscuity for native and non-native diterpenoids, highlights the potential of these P450s for natural product engineering.

Introduction

Diverse networks of specialized metabolites impact plant fitness by mediating ecological interactions among plants, microbes and animals. Among these metabolites, diterpenoids play essential roles in plant defense and ecological adaptation (Tholl, 2015). For instance, chemically distinct diterpenoid blends confer pathogen and pest resistance in major global grain crops, including maize (*Zea mays*) and rice (*Oryza sativa*) (Schmelz et al., 2014; Murphy and Zerbe, 2020). Recent studies further suggest diterpenoid functions in mediating abiotic stress adaptation. For example, UV irradiation elicited diterpenoid accumulation and expression of the corresponding metabolic genes in rice (Park et al., 2013; Horie et al., 2015). Inducible diterpenoid formation was also observed in maize in response to oxidative, drought and salinity stress (Vaughan et al., 2014; Christensen et al., 2018; Mafu et al., 2018), and diterpenoid-deficient maize mutants show decreased resilience to abiotic perturbations (Vaughan et al., 2015). Expanding knowledge of diterpenoid diversity, associated metabolic pathways and functions across a broader range of monocot crop species can inform adaptive breeding and engineering strategies to improve crop environmental resilience (Bevan et al., 2017; Nelson et al., 2018; Bailey-Serres et al., 2019).

Switchgrass (*Panicum virgatum*) is a key species of the North American tallgrass prairie ecosystem and valued as a forage and biofuel crop for its high net energy yield and abiotic stress tolerance (Schmer et al., 2008; Liu et al., 2015; Lovell et al., 2021). Broad drought-induced alterations in carbohydrate, lipid, phenylpropanoid and terpenoid metabolism support a role of

specialized metabolites in switchgrass abiotic stress resilience (Xingxing Li; Meyer et al., 2014; Pelot et al., 2018; Muchlinski et al., 2019).

Diterpenoids in monocot crops almost invariably belong to the group of labdane-type metabolites, and feature species-specific structures, bioactivities, and spatiotemporal regulation and distribution (Schmelz et al., 2014; Murphy and Zerbe, 2020). Diterpene synthases (diTPS) and cytochrome P450 monooxygenases (P450) are the key gatekeepers to diterpenoid diversity (Zerbe and Bohlmann, 2015; Banerjee and Hamberger, 2018). Rooted in the common C20 precursor, geranylgeranyl pyrophosphate (GGPP), the conserved pathway architecture en route to labdane diterpenoids recruits the combined activity of class II and class I diTPSs. After class II diTPS catalyzed conversion of GGPP into bicyclic prenyl pyrophosphate compounds of distinct stereochemistry and oxygenation, class I diTPSs facilitate the dephosphorylation and subsequent cyclization and/or rearrangement of these intermediates to generate various diterpenoid scaffolds (Peters, 2010). Functional decoration through the activity of P450s and other modifying enzyme classes then expands the structural complexity and bioactivity of plant diterpenoids (Banerjee and Hamberger, 2018). Over the past decades, numerous diterpenoid-metabolic diTPSs and P450s have been identified in maize, rice and wheat (*Triticum aestivum*) (reviewed in Schmelz et al., 2014; Murphy and Zerbe, 2020), and demonstrated that downstream of the central GGPP precursor, labdane diterpenoid biosynthesis is organized as modular metabolic networks, where pairwise reactions of functionally distinct enzymes create multiple pathway branches to readily increase product diversity (Xu et al., 2007; Morrone et al., 2011; Mafu et al., 2018; Murphy et al., 2018; Ding et al., 2019). By integrating genome-wide pathway discovery and combinatorial protein biochemical tools, our prior work identified a large and

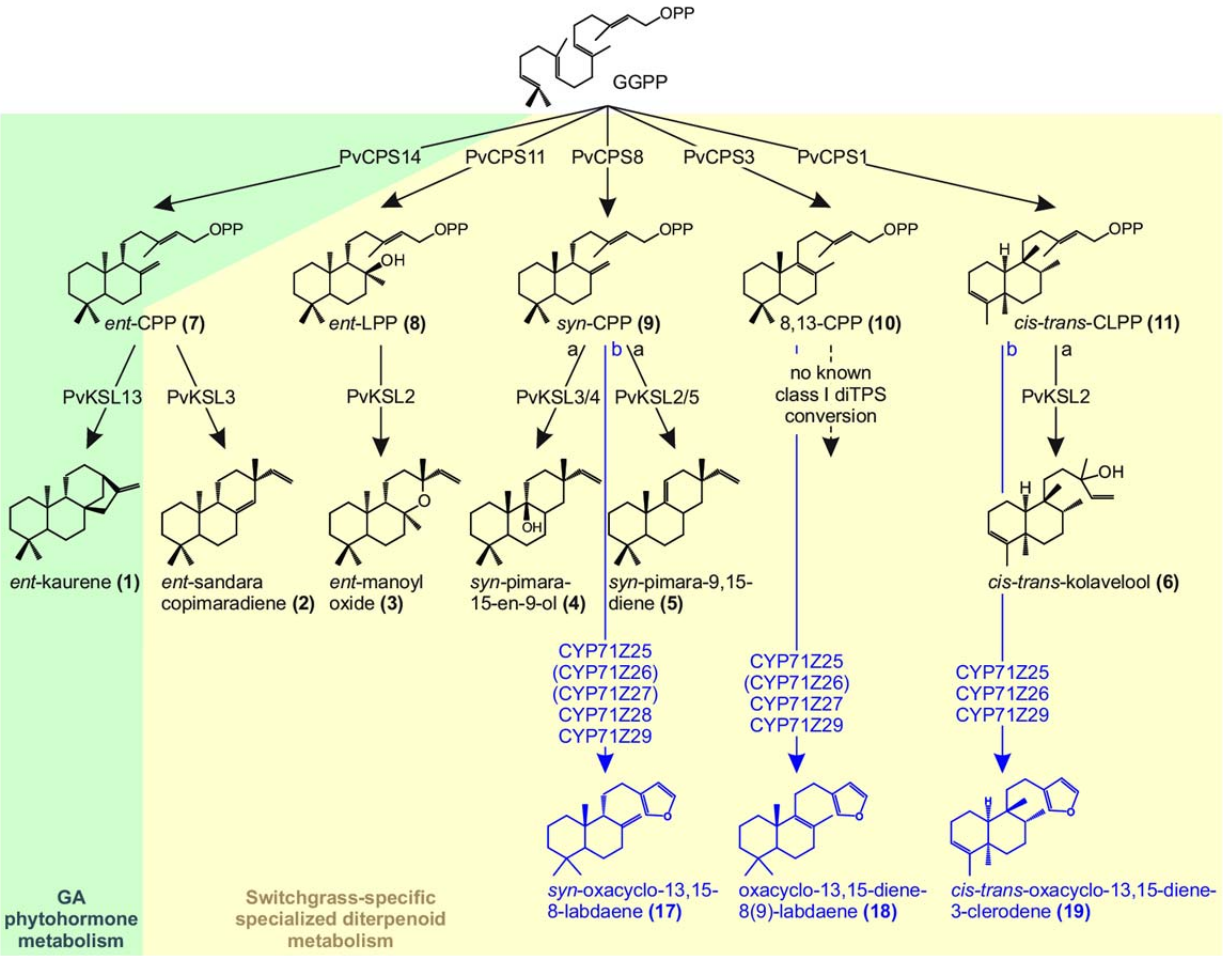

Figure 1. Switchgrass diterpenoid-metabolic network. Shown is an overview of identified biosynthetic pathways, involving monofunctional class II and class I diTPSs, as well as P450 enzymes (this study) that convert the central precursor GGPP into a range of diterpenoid metabolites with putative roles in general (gibberellin phytohormone; green) and specialized (yellow) diterpenoid metabolism.

diverse diTPS family in switchgrass (*Panicum virgatum*) (Pelot et al., 2018) that yields an expansive diversity of diterpenoids, including several labdane-type compounds that occur, to current knowledge, uniquely in switchgrass (Pelot et al., 2018) (Fig. 1). Endogenous accumulation of several metabolites and expression of the corresponding biosynthetic genes in roots and leaves following abiotic stress support a role of terpenoids in switchgrass environmental adaptation (Pelot et al., 2018; Muchlinski et al., 2019); however, complete metabolic pathways, products, and their physiological functions remain to be resolved.

125 Combining genomic studies, combinatorial enzyme assays, metabolite and transcript
126 profiling, and protein structure-function studies revealed a group of five P450s of the CYP71
127 clan (CYP71Z25-29) that convert a range of diterpene scaffolds into furanoditerpenoid
128 derivatives. P450-catalyzed addition of a furan ring directly to diterpene alcohol intermediates
129 derived from class II diTPS activity illustrates a previously unrecognized alternative to the
130 common labdane diterpenoid formation requiring pairwise class II and class I diTPS activity. Co-
131 expression of functionally compatible *diTPSs* and *P450s* in switchgrass roots and drought-
132 elicited accumulation of select diterpenoids support a role in abiotic stress responses.
133 Mechanistic insight into CYP71Z25-29 catalysis enables resources for engineering a broad range
134 of bioactive furanoditerpenoids.
135
136

Results

Identification of diterpenoid-metabolic P450s in the switchgrass genome

To elucidate P450 pathways for the functional decoration of the expansive spectrum of diterpenoid structures in switchgrass, we probed the genomic regions neighboring known switchgrass *diTPS* genes (*P. virgatum*; var. Alamo AP13; genome version v5.1) (Lovell et al., 2021, Pelot et al., 2018). A tandem pair of two *P450* genes, designated *CYP71Z26* (*Pavir.1KG382300*) and *CYP71Z27* (*Pavir.1KG382400*), co-localized on chromosome 1K in direct proximity to three class II *diTPS* genes, including the *cis-trans*-clerodienyl pyrophosphate (*cis-trans*-CLPP) synthase *PvCPS1* (*Pavir.1KG382200*) (12.5 kb and 43.5 kb, respectively), its paralog *PvCPS2* (*Pavir.1KG382115*), and an additional putative *diTPS* (*Pavir.1KG382110*) (Fig. 2A). An additional P450 candidate, *CYP71Z25* (*Pavir.1KG341400*), was identified distantly (1.3 Mb from *CYP71Z27*) on chromosome 1K. Orthology networks including the genomes of switchgrass, the diploid switchgrass relative *P. hallii* (DOE-JGI) (Lovell et al., 2018), and *Setaria italica* (Bennetzen et al., 2012) identified five additional switchgrass P450s, while only one in *S. italica* and two possible paralogs in *P. hallii* were observed (Fig. S1). Notably, the paralogs, *Pahal.A02218* and *Pahal.A02220*, were also clustered in the genome of *P. hallii* (var. filipes FIL2; version v2.0) (Lovell et al., 2018) and co-localized with two class II diTPSs, *Pahal.A02215* and *Pahal.A02217*, with predicted *cis-trans*-CLPP and 8,13-CPP synthase activities, respectively (Pelot et al., 2018) (Fig. 2B). Among the remaining identified switchgrass candidates, only two, *CYP71Z28* (*Pavir.1NG304500*) and *CYP71Z29* (*Pavir.1NG309700*), represented full-length open reading frames and are located distantly (~552 kb) from each other on chromosome 1N (Fig. 2A). CYP71Z25-29 showed high protein sequence identity (90-99%) among the five switchgrass proteins and 82-91% to the two *P. hallii* homologs (Fig. 2C, Fig. S1).

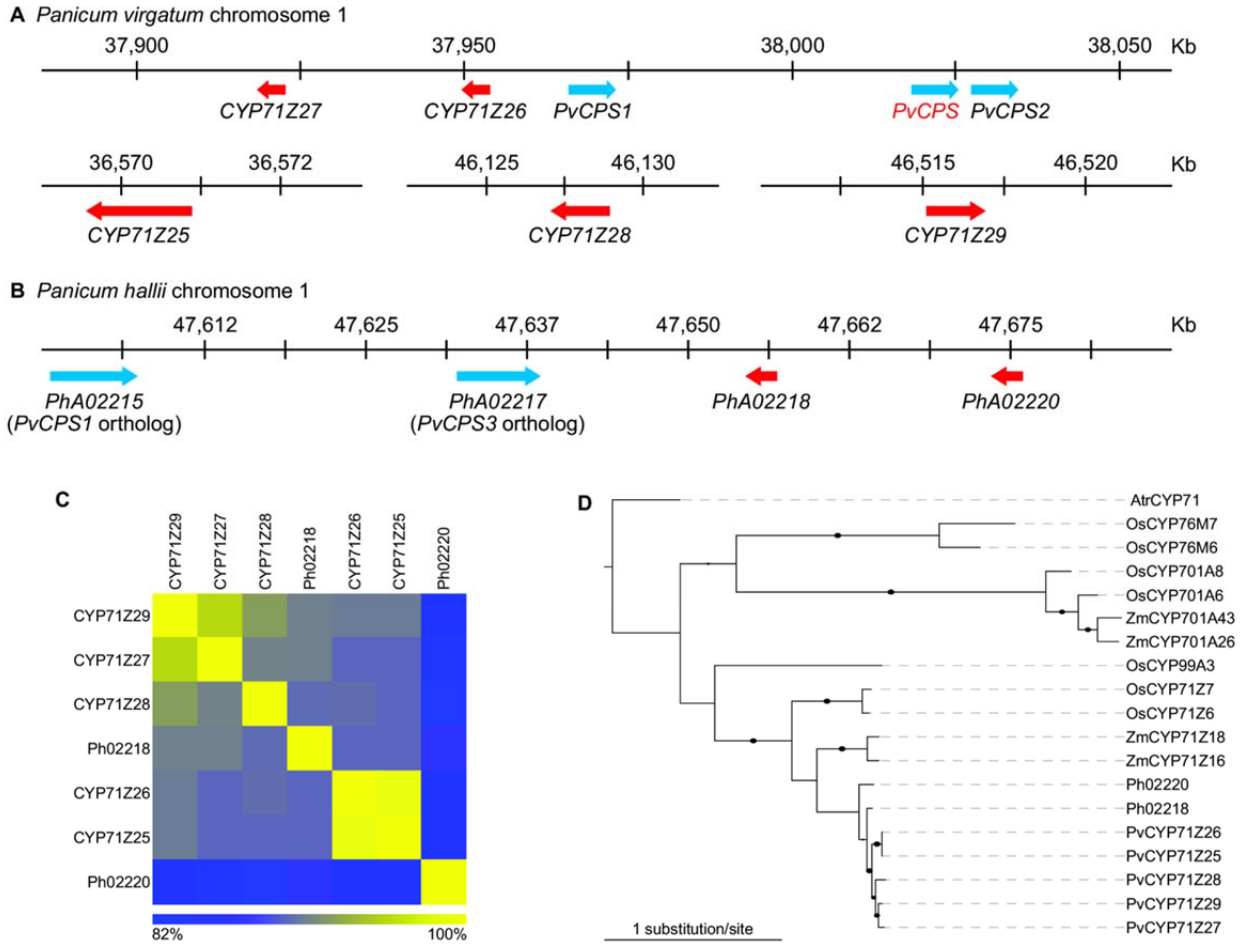

Figure 2. Discovery of switchgrass (Panicum virgatum) cytochrome P450 monooxygenases. (**A-B**) Genomic co-location of P450 genes (red) with class II diterpene synthases (blue) in the *P. virgatum* (var. Alamo AP13) genome (version v5.1) and the genome of the diploid switchgrass relative *P. hallii* (var. filipes FIL2, version v3.1) (DOE-JGI(b); Lovell et al., 2018). (**C**) Heat map illustrating the amino acid sequence identity of the five identified switchgrass P450 candidates, CYP71Z25-29, and orthologous P450s from the diploid switchgrass relative *P. hallii*. (**D**) Maximum-likelihood phylogenetic tree of CYP71Z25-29 with predicted or characterized diterpenoid-metabolic P450s from other monocot crops (Table S4). Tree rooted with the uncharacterized CYP71 from *Amborella trichopoda*. Branches with bootstrap support greater than 80% (500 repetitions) are depicted by black circles.

Phylogenetic analysis with characterized diterpenoid-metabolic P450s from related Poaceae species placed the switchgrass proteins in a distinct clade together with the *P. hallii* (Fig. 2D). This branch showed the closest relationship with members of the CYP71 clan with known roles in specialized diterpenoid metabolism in maize and rice (Wu et al., 2011; Mao et al., 2016; Mafu et al., 2018; Ding et al., 2019), thus indicating related, yet distinct functionalities.

Switchgrass CYP71Z enzymes form distinct furanoditerpenoids

To functionally characterize the identified switchgrass P450s (CYP71Z25-29), we employed combinatorial pathway reconstruction assays of codon-optimized, N-terminally modified P450 constructs with functionally distinct diTPSs and a maize cytochrome P450 reductase (*Zm*CPR2) using an established *E. coli* expression platform (Morrone et al., 2010; Murphy et al., 2019). Following the typical pathway organization of plant labdane diterpenoid metabolism (Peters, 2010), we first tested the co-expression of each P450 with different pairs of class II and class I diTPSs that produce six core diterpenoid scaffolds formed by the switchgrass diTPS family (Pelot et al., 2018), namely *ent*-kaurene **1** (derived from *ent*-copalyl pyrophosphate, CPP **7**), *ent*-sandaracopimaradiene **2** (derived from **7**), *ent*-manoyl oxide **3** (derived from *ent*-labdadienol pyrophosphate, LPP **8**), *syn*-pimara-15-en-9-ol **4** (derived from *syn*-CPP **9**), *syn*-pimara-9,15-diene **5** (derived from **9**), and *cis-trans*-kolavelool **6** (derived from *cis-trans*-clerodienyl pyrophosphate, CLPP **11**). For compound numbering and structures see Fig. 1 & Fig. S2. When compared to the products of the combined class II and class I diTPS activity alone, trace amounts of P450 products were detected only for CYP71Z25, CYP71Z26, and CYP71Z29 when co-expressed with *Pv*CPS1 and *Pv*KSL2 that form **11** and **6**, respectively (Fig. 3A; Fig. S3). The respective P450 products featured near identical fragmentation patterns with characteristic mass ions of *m*/*z* 286, 191, 177, 95, and 81, indicative of an oxygenated labdane scaffold. Notably, presence of these P450 products when co-expressed with *Pv*CPS1 and *Pv*KSL2 coincided with this diTPS pair yielding the lowest product formation of all tested diTPS combinations, resulting in a higher accumulation of the dephosphorylated *cis-trans*-CLPP 15-hydroxy derivative *cis-trans*-kolavenol **16**, due to the activity of endogenous *E. coli* phosphatases.

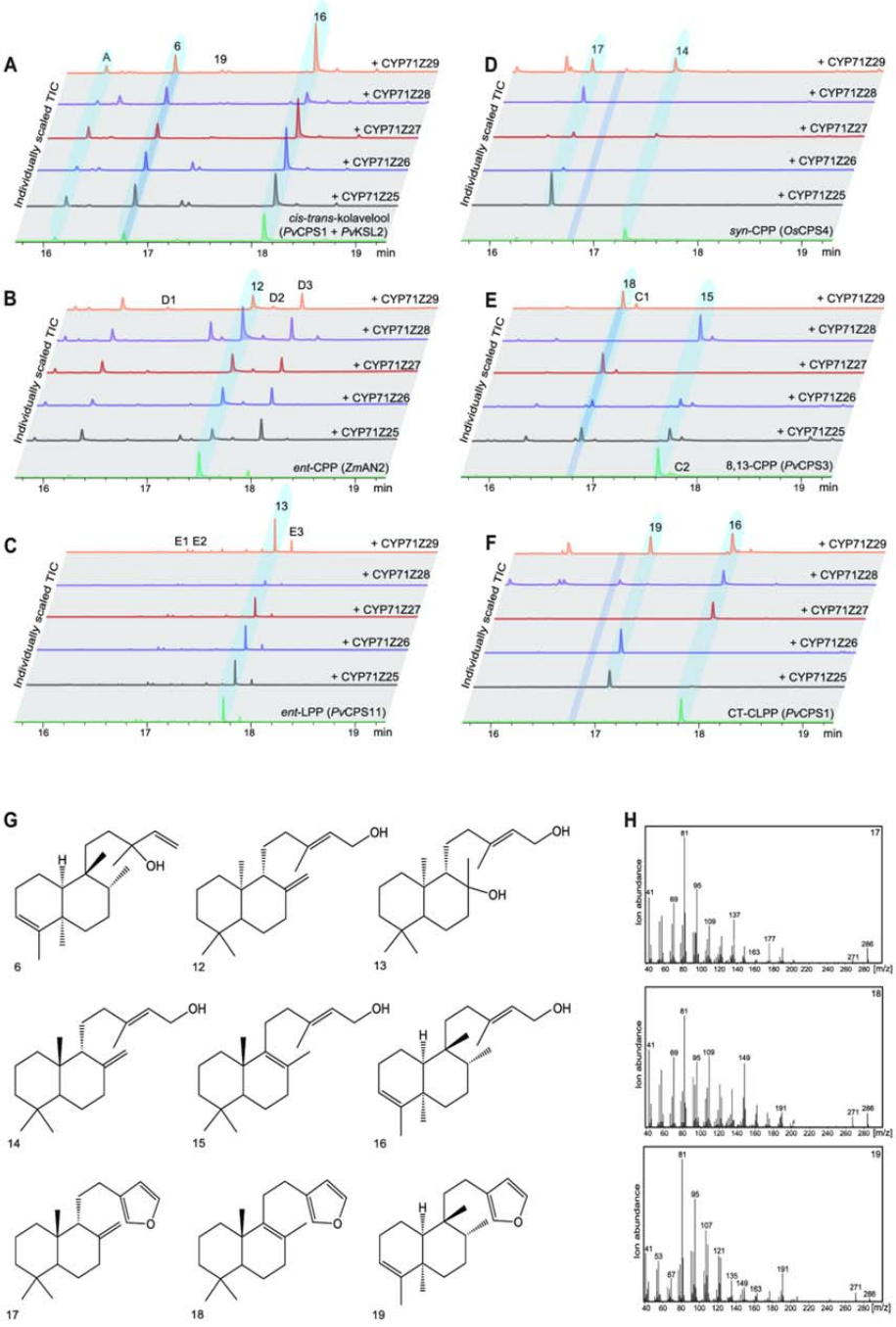

Figure 3. Functional characterization of switchgrass CYP71Z25-29. (**A-F**) Individually scaled total ion GC-MS chromatograms of enzyme products resulting from E. *coli* co-expression of each P450 candidate (CYP71Z25-29) with different diterpene synthases: (**A**) PvCPS1 and PvKSL2 producing the diterpenoid scaffold cis-trans-kolavelool **6**, (**B**) ZmAN2 producing *ent*-copalyl pyrophosphate (CPP) **7**, (**C**) PvCPS11 producing *ent*-labdadienyl pyrophosphate (LPP) **8**, (**D**) *Oryza sativa* CPS4 producing *syn*-CPP **9**, (**E**) PvCPS3 producing 8,13-CPP **10**, and (**F**) PvCPS1 producing *cis-trans*-clerodienyl pyrophosphate (CT-CLPP) **11**. Compounds labeled as C1-2, D1-3 and E1-3 indicate unidentified terpenoid products based on mass spectral patterns. Unlabeled peaks represent non-terpenoid compounds derived from *E. coli* expression cultures. (**G**) Structures of relevant enzyme products. Structures of **17**, **18**, and **19** were verified by NMR analysis and absolute stereochemistry assigned based on the corresponding class II diterpene synthase products. (H) Mass spectra of identified P450 furanoditerpenoid products.

188 This result, in conjunction with the genomic co-localization of several P450 candidates with

189 *PvCPS1* or *PvCPS2*, supported the hypothesis that CYP71Z25-29 function in combination with
190 only class II diTPSs. To test this hypothesis, *E. coli* co-expression assays were conducted pairing
191 each P450 candidate with individual class II diTPSs producing the distinct prenyl pyrophosphate
192 products known in switchgrass: **7**, **8**, **9**, **11** and 8,13-CPP **10** (Pelot et al., 2018) (Fig. S2). GC-
193 MS analysis of the respective reaction products showed product formation by all P450s, although
194 with apparent differences in substrate specificity (Fig. 3B-F). It should be noted that GC-MS
195 analysis detected the dephosphorylated class II diTPS products due to the activity of endogenous
196 *E. coli* phosphatases (*ent*-copalol **12**, *ent*-labdadienol **13**, *syn*-copalol **14**, 8,13-copalol **15**, and
197 *cis-trans*-kolavenol **16**. No P450 products were observed with **12** or **13** as substrates (Fig. 3B-C).
198 Conversion of **16** was observed for CYP71Z25, CYP71Z26 and CYP71Z29, whereas CYP71Z27
199 and CYP71Z28 showed no activity. Importantly, the resulting P450 product featured the same
200 retention time and a near-identical fragmentation pattern as compared to the product observed
201 when combing the *cis-trans*-CLPP (**11**) synthase *Pv*CPS1 with the *cis-trans*-kolavelool **6**
202 synthase *Pv*KSL2 and a P450 candidate (Fig. 3A,F). Conversion of **15** was observed for
203 CYP71Z27, CYP71Z29, and partially for CYP71Z25 and CYP71Z26, whereas CYP71Z28 was
204 largely inactive with this substrate (Fig. 3E). By contrast, CYP71Z28 showed high activity with
205 **14** as a substrate, as did CYP71Z25 and CYP71Z26, whereas CYP71Z27 and CYP71Z29
206 showed only incomplete substrate conversion (Fig. 3D). For all observed P450 products,
207 fragmentation patterns featured *m/z* 286, 191, and 177 mass ions consistent with oxygenated
208 labdane diterpenoid structures (Fig. 3G-H).

209 To determine the structure of selected P450 products, enzymatically produced and purified
210 compounds were subject to 1D and 2D NMR (HSQC, COSY, HMBC and NOESY) analysis and
211 compared to previously reported NMR data where available. This approach revealed a shared

structural scaffold of the P450 products that contains the individual class II diTPS-derived diterpene backbones with a furan ring addition at the C15-C16 position (Fig. 3G). Furanoditerpenoid products identified here included *syn*-15,16-epoxy-8(17),13(16),14-triene **17** derived from the *Pv*CPS8 product **14** (Fig. S4), 15,16-epoxy-8,13(16),14-triene **18** derived from the *Pv*CPS3 product **15** (Fig. S5), and *cis-trans*-15,16-epoxy-cleroda-3,13(16),14-triene **19** derived from the *Pv*CPS1 product **16** (Fig. S6). The stereochemistry of the P450 products was assigned on the basis of the respective class II diTPS products (Pelot et al., 2018).

Considering the substrate promiscuity of CYP71Z25-29, we next investigated the capacity of these P450s to convert alternate class II diTPS products. Indeed, with the exception of CYP71Z28, all P450s formed (+)-15,16epoxy-8(17),13(16),14-triene **26** when co-expressed with a diTPS producing (+)-CPP **20** ((+)-copalol **23**), a class II diTPS product not currently known in switchgrass, but formed by diTPSs of other monocot crops such as wheat and maize (Wu et al., 2012; Murphy et al., 2018) (Figs. S7 and S8). In addition, CYP71Z25 and CYP71Z26 showed, albeit low, activity when co-expressed with the *trans-cis*-neo-clerodienyl pyrophosphate (*trans-cis*-CLPP **22**; *trans-cis*-kolavenol **25**) synthase of *Salvia divinorum*, *Sd*CPS2 (Pelot et al., 2017), forming the core precursor to salvinorin A, a neoclerodane furanoditerpenoid with potential use for the treatment of drug addiction and neuropsychiatric disorders (Kivell et al., 2014). The two major P450 products showed signature mass ions of *m*/*z* 286 or *m*/*z* 288, indicating a **25**-derived furanoditerpenoid **28** and *trans-cis*-cleroda-3,12-dien-15,16-diol **29** structures, respectively (Fig. S7).

Formation of furanoditerpenoids through the coupled activity of the focal P450s and functionally distinct class II diTPSs warranted a deeper investigation of the nature of the P450 substrate. While class II diTPSs form prenyl pyrophosphate products with a characteristic

pyrophosphate group at C15 (Peters, 2010), as mentioned above, expression of class II diTPSs in heterologous plant or microbial host systems typically yields the corresponding C15-hydroxy derivatives formed through the activity of endogenous phosphatases (Mafu et al., 2018; Pelot et al., 2018; Ding et al., 2019). To clarify the catalytic preference of CYP71Z25-29, substrate feeding experiments were conducted by adding enzymatically produced and purified compounds of **15** or **16** to *E. coli* cultures expressing CYP71Z25 or CYP71Z29. For both tested P450-substrate combinations, conversion of the 15-hydroxy diterpene substrates into the respective furanoditerpenoids was observed, whereas no conversion was detected in control samples expressing plasmids carrying *Zm*CPR2 alone (Fig. S9). Substantial limitations in purifying the corresponding prenyl pyrophosphate compounds prevented the possibility to conduct complementary feeding assays within the scope of this study.

Structure-guided mutagenesis identifies active site determinants of P450 catalytic specificity

To investigate the catalytic mechanism underlying the unusual activity of CYP71Z25-29, homology models were generated for each P450 using the recently reported crystal structure of *Salvia miltiorrhiza* CYP76AH1 (Gu et al., 2019) as a template. Given a protein identity of only ~ 42% to the target P450s (Fig. S10), an iterative homology modeling and energy minimization approach employing relaxed template protein structures (Nivón et al., 2013; Pei and Grishin, 2014) was used to generate high-quality models. The resulting lowest energy model was used for ligand docking of the heme co-factor into the individual active sites. The generated structural models showed root-mean-square deviation (RMSD) values of 0.67-0.75 as compared to the template, thus representing high-quality reproduction of common secondary structures and placement of active site residues as demonstrated, for example, for the heme-anchoring cysteine

C421 (Fig. S10). The five diterpenoid substrates tested in this study were then docked into the heme-model complex with three conceivable substitution arrangements: 15-hydroxy and 15-pyrophosphate structures as alternate substrates and 15,16-dihydroxy derivatives as intermediate or product of the P450-catalyzed oxygenation reaction (Figs. S2 and S10). Comparison of the interaction energy (IE) of all generated substrate-P450 docking poses showed that the average IE was most favorable for the 15-hydroxy and 15-16-dihydroxy substrates, whereas the 15-pyrophosphate structure was energetically less favorable (Table S1). The difference in IE between the 15-hydroxy and 15-pyrophosphate ligands can presumably be attributed to the far larger volume and electrostatic charge of the pyrophosphate moiety.

The various modeled substrate-protein complexes were then used to investigate active site residues with possible impact on the distinct substrate specificity of CYP71Z25-29. A total of 15 active site residues associated with the six known CYP71 substrate recognition sites (SRS) (Dueholm et al., 2015) were identified that were located proximal to the docked substrates and showed residue variation among CYP71Z25-29 and related members of the CYP71Z subfamily (Fig. 4A). To investigate the catalytic impact of these residues, protein variants of CYP71Z25 and CYP71Z27, as the functionally most contrasting P450s, were generated via site-directed mutagenesis and functionally characterized by *E. coli* co-expression with individual class II diTPSs producing native (**14**, **15**, **16**) or non-native (**23**, **24**, **25**) P450 substrates. Reciprocal mutagenesis of all 15 identified residues between CYP71Z25 and CYP71Z27 (F/Y81, F/S86, V/I89, N/D95, S/T187, L/Q188, A/G215, V/Y218, R/Q220, V/L226, E/D283, T/I288, L/M293, S/T346, M/I463) resulted in a near-complete loss of function of the corresponding CYP71Z25 variant (Fig. 4B, Fig. S10). By contrast, the reciprocal multi-residue variant of CYP71Z27 featured an altered product profile largely reflecting the wild type products of CYP71Z25.

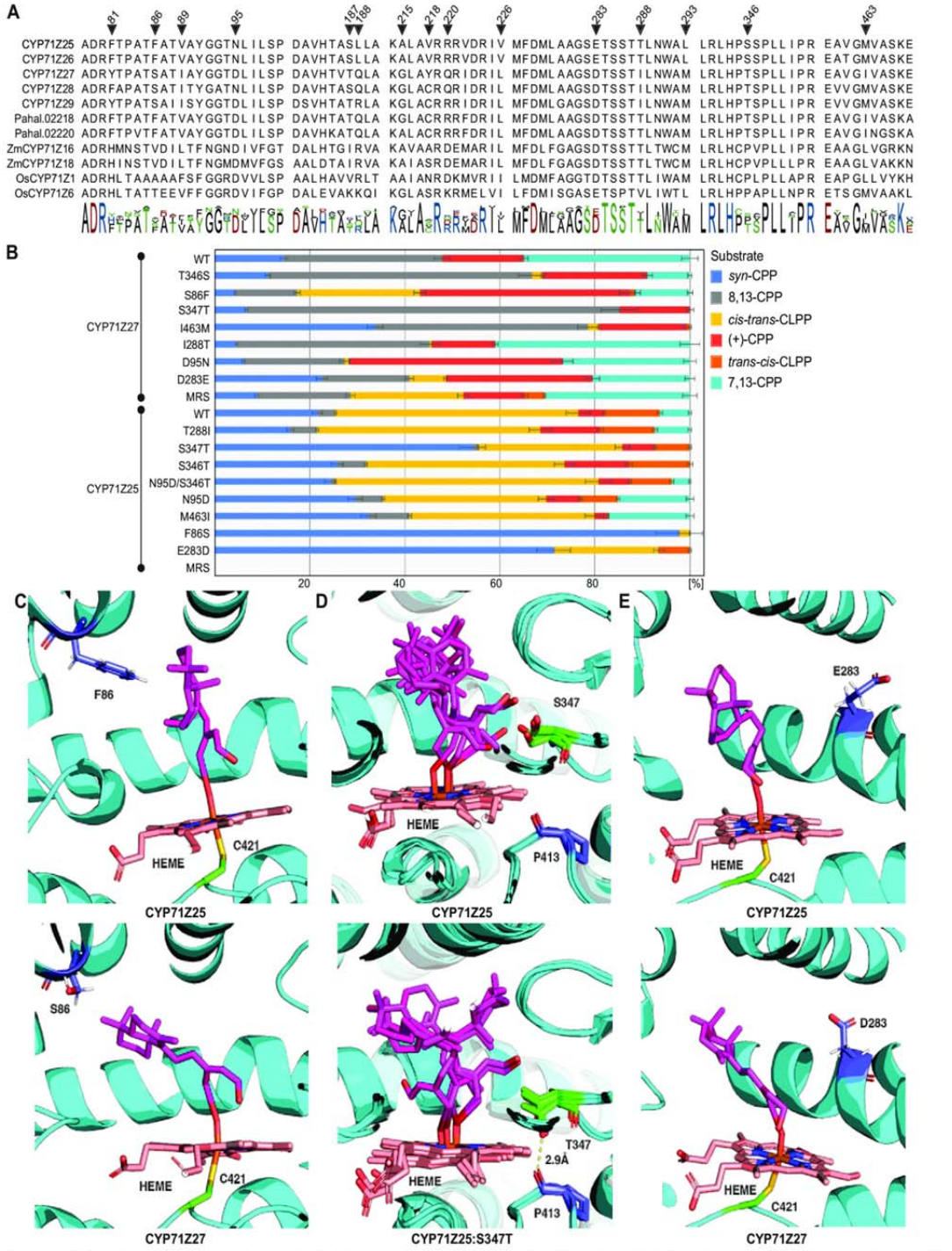

Figure 4. (**A**) Protein sequence alignment of Substrate Recognition Site (SRS) motifs of CYP71Z25-29 and related members of the CYP71Z subfamily of known or predicted function. (**B**) Analysis of standardized substrate conversion by CYP71Z25 and CYP71Z27 SDM variants. *E. coli* co-expressions for each variant with native (14, 15, 16) and non-native (23, 24, 25) switchgrass substrates were carried out in triplicate and normalized to the internal standard 1-eicosane and the OD600 at time of induction of protein expression. Error bars indicate standard deviation of replicates from the mean. (**C**) Active sites of CYP71Z25 (right) and CYP71Z27 (left) with heme (magenta), substrate (pink), and residues C412 (green) and S/F86 (blue). (**D**) Structural overlay of the five lowest IE active sites of CYP71Z25 (left) and CYP71Z25-S347T variant (right) with 15 (8,13-copalol) substrate (pink) and heme (magenta) docked. Residues S/T347 (green), P413 (blue), and corresponding hydrogen bonding (yellow dashes) with distance in Ångstrom are highlighted. (**E**) Active sites of CYP71Z25 (right) and CYP71Z27 (left) with heme (magenta), substrate (pink), and residues C412 (green) and E/D283 (blue).

281 Strikingly, the single residue variant CYP71Z27:S86F showed a product profile similar to that

observed for the multi-residue variant of CYP71Z27, converting all six tested diterpene alcohol substrates (Fig. 4B,C). By contrast, the reciprocal CYP71Z25:F86S variant showed only trace product amounts, again comparable to the multi-residue variant of CYP71Z25. Most notably, this protein variant showed substantial activity in producing **19** making up 23.7±0.6% of the product profile. Analysis of additional single residue variants revealed S347 hydrogen bonds with the docked hydroxy substrates and is conserved in CYP71Z25-29 (Fig. 4A,D). Substitution of S347 for a Thr impaired enzyme activity in CYP71Z27 with the exception of the conversion of 8,13-CPP-derived diterpene alcohols, whereas the same mutation had a lesser impact on CYP71Z25 catalysis reducing predominantly the conversion of **15** by 2.6% and **24** by 6.4% (Fig. 4B). Consistent with the observed protein variant activities, docking of the **15**-derived substrate into the active site crevice of CYP71Z25 and the corresponding S347T variant suggests that exchange of the native S347 residue to a Thr results in hydrogen bond formation with a neighboring Pro residue (P413), rather than the hydrogen bond formed with the substrate in the wild type enzymes (Fig. 4D). Reciprocal exchange of residues E/D283 significantly reduced product formation in CYP71Z25, especially with regards to the conversion of **15**, **23**, **24** (Fig. 4B,E), whereas the corresponding variant CYP71Z27:D283E showed only minor product changes with **19** as an additional product contributing 7.7±0.1% to the profile.

Mutagenesis of the remaining selected residues in CYP71Z25 and CYP71Z27, namely N/D95, T/I288, S/T346 and M/I463, showed limited impact on P450 catalytic specificity, including the formation of **19** as a product absent in the wild type enzyme by the CYP71Z27:D95N and CYP71Z27:T346S variants. Furthermore, the CYP71Z25:T288I variant and an additional double mutation, CYP71Z25:N95D/S346T showed a 9% increase in producing **28** when co-expressed with the *trans-cis*-CLPP synthase *Sd*CPS2 (Fig. S4).

P450-derived furanoditerpenoids show drought-elicited formation in switchgrass roots

Previous work demonstrated that select diTPS transcripts and corresponding enzyme products, including **3** and **4**, accumulate in switchgrass (Alamo) leaves and roots exposed to below-ground oxidative stress (Pelot et al., 2018). To determine if furanoditerpenoid biosynthesis follows similar patterns, we examined P450-derived furanoditerpenoids in switchgrass plants exposed to four weeks of drought stress. Targeted GC-MS metabolite profiling of organic solvent extracts of droughted switchgrass roots and well-watered control plants illustrated an, albeit moderate, accumulation of several diterpenoid compounds, including **4**, a yet unidentified diterpenoid, and two metabolites, **30** and **31**, that show mass fragmentation patterns significantly similar but distinct from the identified furanoditerpenoid P450 products, suggesting that these compounds may represent further functionalized derivatives (Fig. 5A&B, Fig. S11). Specifically, mass ions of *m*/*z* 177 and *m*/*z* 192 indicated a *syn*-labdane backbone of compound **30**. Compound **31** featured a prominent *m*/*z* 148 possibly indicating an 8,13-labdane scaffold, as well as a *m*/*z* 304 mass fragment suggesting that this compound carries an additional hydroxy group (Fig. 5B). Low abundance of the identified diterpenoids prevented their purification from plant material for structural verification. Notably, all identified diterpenoids were present in both droughted and control plants with only compound **31** showing a moderate accumulation during the course of the drought treatment (Fig. S11).

Additional differential gene expression analysis using the same tissue samples was used to assess *diTPS* and *P450* gene expression patterns in droughted and control leaf and root tissue (Fig. 5B). Gene expression of *CYP71Z25-29* and the majority of diterpenoid-metabolic diTPSs, including the *cis-trans*-CLPP synthase *PvCPS1*, the predicted *syn*-CPP synthases *PvCPS9* and

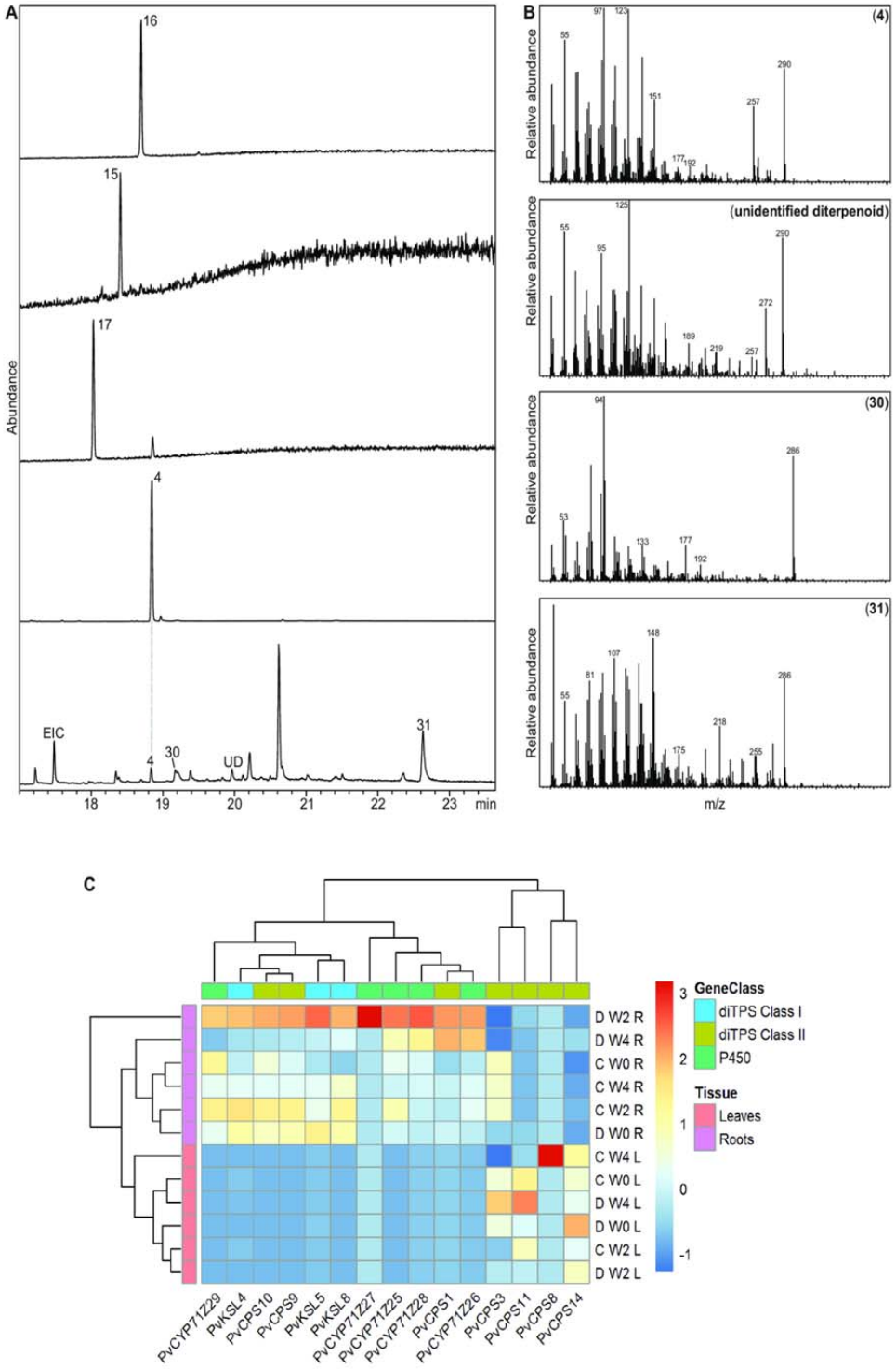

Figure 5. GC-MS total ion chromatograms (**A**) and mass spectra (**B**) of diterpenoids detected in organic solvent extracts of switchgrass roots identified diterpenoids **4**, an unidentified diterpenoid (UD) and predicted furanoditerpenoids (compounds 30 and 31) as possible derivatives of products of CYP71Z25-29. (**C**) Hierarchical cluster analysis of select diTPS and CYP71Z25-29 gene expression profiles from drought stressed tissues. Samples were collected before starting treatment (W0), two weeks (W2), and four weeks (W4) of drought stress treatment. L=leaves, R=roots, Drought stressed=D, well-watered=C.

328 *PvCPS10* and the downstream-acting class I *diTPS PvKSL4*, *PvKSL5*, and *PvKSL8*, was detected

329 only in roots consistent with the presence of compound **4** and predicted furanoditerpenoids. By
330 contrast, the 8,13-CPP (**10**) synthase *PvCPS3* was moderately expressed in both organs, whereas
331 the *ent*-LPP (**8**) synthase *PvCPS11* and the putatively gibberellin-biosynthetic *ent*-CPP (**7**)
332 synthase *PvCPS14* were expressed only in leaves. Distinct from its homologs, *PvCPS9* and
333 *PvCPS10*, the *syn*-CPP (**9**) synthase *PvCPS8* was expressed only in leaves after four weeks of
334 treatment in well-watered plants, suggesting an expression profile at only later developmental
335 stages. Drought-induced gene expression of root-specific specialized *diTPSs* and *CYP71Z25-29*
336 was observed to be moderate with an increase until two weeks of drought treatment, followed by
337 a decreased transcript abundance at four weeks of treatment (Fig. 5B). In leaves, expression of
338 the specialized class II *diTPSs PvCPS3* and *PvCPS11* was highest after four weeks of drought
339 treatment, whereas *PvCPS8* showed no drought-elicited transcript accumulation.
340
341

Discussion

Crop improvement strategies increasingly benefit from knowledge of gene-to-metabolite relationships that contribute to desired crop traits and serve as resources for molecular crop engineering or breeding (Jez et al., 2016). Particularly, knowledge of the dynamic networks of plant specialized metabolites that enable plants to adapt to environmental pressures is needed in light of exacerbating crop losses caused by climate shifts and associated pest and disease damage (Savary et al., 2019). Diterpenoids serve as key components of biotic and abiotic stress resilience in rice and maize (Schmelz et al., 2014; Murphy and Zerbe, 2020), and stress-inducible, species-specific diterpenoid networks have also been discovered in other food and bioenergy crops such as switchgrass, foxtail millet and wheat, although their physiological functions are less well understood (Wu et al., 2012; Zhou et al., 2012; Schmelz et al., 2014; Pelot et al., 2018; Ding et al., 2019; Karunanithi et al., 2020). Prior studies identified an expansive *diTPS* gene family in allotetraploid switchgrass that forms specialized diterpenoids both common among the grass family and, to current knowledge, uniquely present in switchgrass (Pelot et al., 2018). The discovery of a group of functional *P450* genes, *CYP71Z25-29*, that function as furanoditerpenoid synthases via an alternate pathway independent of class I diTPS activity provides a deeper understanding of the divergence of switchgrass diterpenoid metabolism and how the natural modularity of diterpenoid-biosynthetic pathways drives the evolution of complex, lineage-specific blends of bioactive metabolites.

Identification of eight *CYP71Z*-type genes in switchgrass, as compared to only one paralog in *S. italica* and two genes in the diploid switchgrass relative *P. hallii*, suggests an expansion of this P450 group after the split from *P. hallii* approximately 8 MYA (Lovell et al., 2021). A close phylogenetic relationship among the functional members, CYP71Z25-29, indicates a shared

365 evolutionary origin preceding gene duplication and sub/neo-functionalization events common in
366 diterpenoid pathway evolution (Zi et al., 2014). Localization of *CYP71Z26* and *CYP71Z27* on
367 chromosome 1K, along with a near-identical gene arrangement of two paralogs in *P. hallii*,
368 whereas *CYP71Z25*, *CYP71Z28* and *CYP71Z29* are located on subgenome K, suggests that gene
369 family expansion was associated with switchgrass subgenome expansion approximately 4.6
370 MYA (Lovell et al., 2021).

371 Diterpenoid-forming members of the CYP71Z subfamily also exist in maize and rice, where
372 they catalyze position-specific hydroxylation, carboxylation or epoxidation reactions in various
373 labdane scaffolds produced by the pairwise activity of class II and class I diTPS enzymes (Wu et
374 al., 2011; Mafu et al., 2018; Ding et al., 2019). Consistent with their phylogenetic distance from
375 maize and rice CYP71Z enzymes, functional characterization of switchgrass CYP71Z25-29
376 demonstrated a rare P450 activity in catalyzing the addition of a furan ring at C15-C16 of a range
377 of different labdane scaffolds. The only known example of P450-mediated furan ring formation
378 is the biosynthesis of the monoterpenoid menthofuran catalyzed by CYP71A32 in members of
379 the *Mentha* genus (Bertea et al., 2001). Strikingly, contrasting known labdane diterpenoid
380 pathways that invariably require the activity of class II and class I diTPSs, CYP71Z25-29
381 showed no detectable activity in converting class I diTPS products. Instead, efficient
382 furanoditerpenoid synthase activity of CYP71Z25-29 was observed in co-expression assays with
383 class II diTPSs alone (Fig. 3). Feeding assays with 15-hydroxy derivatives of select class II
384 diTPS products illustrate that these diterpene alcohols rather than the 15-pyrophosphate
385 compounds are the preferred CYP71Z25-29 substrates. This substrate preference is further
386 supported by molecular ligand docking studies showing favorable interaction energies for 15-
387 hydroxy and 15,16-dihydroxy intermediates as compared to the corresponding pyrophosphate

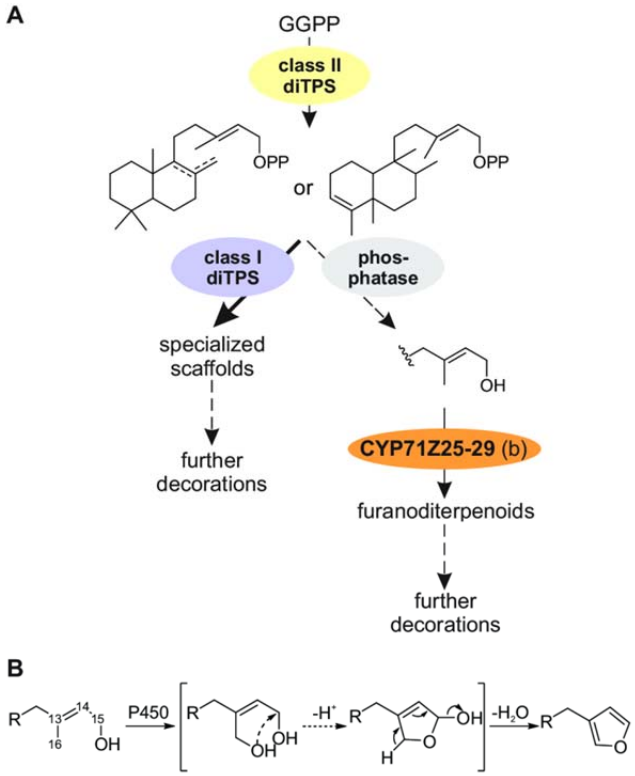

Figure 6. (**A**) Scheme of the postulated formation of diterpenoids in switchgrass. Derived from the common precursor geranylgeranyl pyrophosphate (GGPP) class II diterpene synthase products of different structure and stereochemistry can be formed either by further conversion through class I diterpene synthases and additional possible functional modifications or via cleavage of the pyrophosphate group by yet unidentified phosphatases and conversion of the resulting alcohol intermediates by CYP71Z25-29 to yield different furanoditerpenoids structures. (**B**) Proposed mechanism of furan ring addition catalyzed by CYP71Z25-29 that proceeds through oxidation of the C16 methyl group to form a dihydroxy intermediate, ring closure via deprotonation, and furan ring formation by dehydration.

388 structures. The observed furanoditerpenoid synthase activity of CYP71Z25-29 supports the
389 presence of an alternative labdane diterpenoid pathway route in switchgrass that bypasses the
390 common conversion of class II diTPS products by class I diTPSs and instead involves
391 phosphatase-mediated dephosphorylation and subsequent CYP71Z25-29-catalyzed conversion of
392 the resulting diterpene alcohol intermediates (Fig. 6A). Based on the conversion of the 15-
393 hydroxy labdane substrates by CYP71Z25-29, and similar interaction energies observed for 15-
394 hydroxy and 15,16 dihydroxy labdane intermediates in molecular docking analyses, a catalytic
395 mechanism can be proposed that proceeds through initial substrate hydroxylation at C-16 and
396 subsequent deprotonation and ring closure at C-15, followed by hydride shifts to facilitate

dehydration and formation of the C13-C16 and C14-C15 double bonds (Fig. 6B). Genomic clustering of *CYP71Z25* and *CYP71Z26/27* with the class II diTPSs *PvCPS2* and *PvCPS1,* respectively (Fig. 1A), and co-expression of furanoditerpenoid synthase genes with several class II *diTPS* (including *PvCPS1*) in switchgrass roots (Fig. 5B) further support this hypothesis. While no terpenoid-metabolic plant phosphatases have yet been described, 15-hydroxy derivatives of class II diTPS products are commonly observed in co-expression assays using microbial or *Nicotiana benthamiana* platforms (Morrone et al., 2010; Mafu et al., 2018; Pelot et al., 2018; Ding et al., 2019). Indeed, at least ten predicted acid phosphatase and lipid phosphate phosphatase genes are present in the switchgrass genome (var. Alamo AP13; version v5.1) (Lovell et al., 2021) that are located across chromosomes 1N and 1K.

The primary formation of class I diTPS products rather than furanoditerpenoids when co-expressing class II diTPSs, class I diTPSs and CYP71Z25-29 may suggest that the combined activity of class II and class I diTPSs represents the dominant pathway route. Compartmentalization of plastidial class II and class I diTPSs and common P450 localization at the endoplasmic reticulum supports pairwise diTPS activity as the primary pathway. However, presence of putative furanoditerpenoids derived from the identified P450 products alongside the class I diTPS product **4** and other yet unidentified diterpenoids in switchgrass roots supports the co-occurrence of both pathway branches *in planta*. Co-expression patterns of select biosynthetic genes, including *CYP71Z25/26* as well as *PvKSL4* and *PvKSL5*, relevant for the formation of Syn-CPP-derived diterpenoids in switchgrass roots is consistent with this hypothesis. However, expression of the *syn*-CPP synthase *PvCPS8* only in leaves, may indicate that the predicted functional homologs *PvCPS9* and/or *PvCPS10* are more likely to serve in the biosynthesis of **17** and **4** in roots (Fig. 5B). Given the large size of the switchgrass diTPS family and the catalytic

overlap of CYP71Z25-29, future biochemical and genetic studies will be required to precisely decode the interactions governing the modular formation of switchgrass-specific diterpenoids. Interestingly, the lack of CYP71Z25-29 activity with substrates of *ent*-stereochemistry (including the GA precursor *ent*-CPP) demonstrates a dedicated role of this P450 group in specialized metabolism and highlights a biochemical separation of furanoditerpenoid and general diterpenoid metabolism in switchgrass. Similar impacts of substrate-specificity on partitioning different diterpenoid branches have recently been described in maize, where specificity of two class I diTPSs, *Zm*KSL2 and *Zm*KSL4, for producing distinct positional isomers of *ent*-kaurene contributes to the partitioning of pathways toward dolabralexin and kauralexin diterpenoids (Ding et al., 2019).

Presence of furanoditerpenoids and other specialized diterpenoids (Fig. 5) (Pelot et al., 2018) in switchgrass roots may indicate a role in abiotic stress responses. Albeit at moderate levels, drought-induced gene expression of *CYP71Z25-28* and select *class II diTPS* in roots further supports the association of furanoditerpenoid biosynthesis and switchgrass drought stress responses. Stress-elicited accumulation of diterpenoids with allelopathic and anti-microbial bioactivities in rice roots are well-established (Schmelz et al., 2014), and recent maize studies also demonstrated the root accumulation of diterpenoid dolabralexins and sesquiterpenoid zealexins in response to drought, oxidative and salinity stress (Schmelz et al., 2014; Vaughan et al., 2015; Christensen et al., 2018; Mafu et al., 2018; Murphy and Zerbe, 2020). However, the metabolite abundances detected in switchgrass are lower as compared to stress-elicited terpenoid accumulation in rice and maize. Given the structural distinctiveness of switchgrass diterpenoids, it is conceivable that switchgrass furanoditerpenoids exert different bioactivities in switchgrass interorganismal and environmental interactions. It also appears likely that the detected

443 switchgrass furanoditerpenoids represent lower abundant pathway intermediates that undergo
444 further functional decorations to generate bioactive pathway end products. Indeed, among the
445 approximately 400 known furanoditerpenoids broadly distributed across the plant kingdom, the
446 vast majority feature extensive modifications of both the furan ring and the diterpene skeleton
447 that may include variations of hydroxylation, carboxylation, lactonization, glycosylation and
448 other transformations (Bao et al., 2016).

449 Integrating sequence comparison, molecular dynamics analysis and site-directed
450 mutagenesis proved a powerful tool for identifying active site residues contributing to
451 CYP71Z25-29 catalysis and substrate specificity. The relative ease by which the substrate
452 specificity of CYP71Z25 and CYP71Z27 for labdane intermediates of different stereochemistry
453 and double bond configuration could be altered through minor active site modifications, supports
454 a rapid P450 functional divergence during the evolution of switchgrass diterpenoid metabolism.
455 This is exemplified by a near-complete functional conversion of CYP71Z27 to the product
456 profile of CYP71Z25 with a single S86 to F substitution. However, loss of activity in the
457 reciprocal CYP71Z25 variant suggests that different active site positions play major roles in
458 product specificity among the identified P450s. Indeed, proximity of the F86 aromatic ring to the
459 docked substrate in CYP71Z27 supports a role in substrate orientation in the active site crevice,
460 whereas introduction of a bulky Phe side chain in the CYP71Z25 cavity may lead to steric
461 hindrance of substrate binding and catalysis (Fig. 3C). Further mechanistic insight was gained
462 from substitution of a conserved Ser in the SRS5 domain shown to be imperative for catalysis by
463 hydrogen-bonding to the substrate. Molecular dynamics results suggest that substitution of this
464 position for Thr leads to reduced conformational flexibility and associated side chain rotations
465 that are critical for hydrogen bond formation with the substrate. Paired with the substrate

promiscuity of CYP71Z25-29, these mechanistic insights provide a foundation for producing a broader range of furanoditerpenoid natural products. Notably, many plant furanoditerpenoids have been associated with therapeutic bioactivities ranging from anti-allergic and anti-diabetic to anti-cancer and anti-viral efficacies, whereby the furan group serves as a key pharmacophore (Bao et al., 2016). In this context, the potential of combinatorial pathway reconstruction for diterpenoid manufacturing is highlighted by the capacity of CYP71Z25 and CYP71Z26 to form the corresponding di-hydroxy and furan-derivatives of **25**, the precursor in the biosynthesis of salvinorin A (Pelot et al., 2017), a natural product of *S. divinorum* that was identified as a drug candidate for treatment of drug addictions due to its agonistic activity on brain kappa-opioid receptors (Kivell et al., 2014). Increased catalytic specificity observed in two CYP71Z25 variants further underscores the potential of structure-guided protein engineering for enabling desired P450 activities as more mechanistic insight into diTPS and P450 functions is gained.

Materials and Methods

Gene synthesis

CYP71Z25-29 were synthesized as codon-optimized and N-terminally modified genes by replacement of the sequence upstream of the LPP motif with the leader sequence MAKKTSSKGK (Swaminathan et al., 2009) (Table S2) and individually inserted into MCS2 of a pETDuet-1 vector (www.emdmillipore.com) carrying the full-length, codon-optimized maize cytochrome P450 reductase (*Zm*CPR2) in MCS1. Gene synthesis and cloning were performed by DOE Joint Genome Institute (JGI) with support through a DNA Synthesis Award (#2568). In addition, the multi residue variants of CYP71Z25 and CYP71Z27 were obtained from GenScript (www.genscript.com).

489

490 **_E. coli_ co-expression assays**

491 Co-expression of diTPSs and P450s was conducted in an *E. coli* platform engineered for
492 diterpenoid production (Morrone et al., 2010; Murphy et al., 2019). In brief, pIRS and pGGxC
493 plasmids (Morrone et al., 2010) carrying class II diTPSs with distinct products [*ent*-CPP **7** (*Z.*
494 *mays* AN2; (Harris et al., 2005) used here in place of the native *Pv*CPS14 due to its higher
495 catalytic activity), *syn*-CPP **9** (*O. sativa* CPS4; (Xu et al., 2004) used here in place of the native
496 *Pv*CPS8 due to its higher catalytic activity), (+)-CPP **20** (*Abies grandis* abietadiene synthase
497 variant D621A; (Morrone et al., 2010)), 8,13-CPP **10** (*Pv*CPS3), 7,13-CPP **21** (*Grindelia robusta*
498 7,13-CPP synthase (Zerbe et al., 2015)), *ent*-LPP **8** (*Pv*CPS11), *cis-trans*-CLPP **11** (*Pv*CPS1),
499 *trans-cis*-CLPP **22** (*Salvia divinorum* CPS2; (Pelot et al., 2016) were co-expressed with different
500 P450 genes. For additional co-expression of class I diTPSs, respective genes sub-cloned into the
501 pET28b(+) expression vector were used (Pelot et al., 2018). Constructs were co-transformed into
502 *E. coli* BL21DE3-C43 cells (www.lucigen.com) and cultures were grown at 37°C and 200 rpm
503 in 50 mL Terrific Broth (TB) medium to an OD_{600} of ~0.5-0.6 before cooling to 16°C, and
504 induction with 1 mM isopropyl-β-D-1-thiogalacto-pyranoside (IPTG) and addition of 40 mM
505 sodium pyruvate, 1 mM $MgCl_2$, 5 mg L^{-1} riboflavin and 75 mg L^{-1} 5-aminolevulinic acid. After
506 72 h incubation, metabolites were extracted with hexane and air-dried for GC-MS analysis on an
507 Agilent 7890B GC interfaced with a 5977 Extractor XL MS Detector at 70 eV and 1.2 mL min^{-1}
508 He flow, using an Agilent DB-XLB column (30 m, 250 µm i.d., 0.25 µm film) and the following
509 GC parameters: 50°C for 3 min, 15°C min^{-1} to 300°C, hold 3 min with pulsed splitless injection
510 at 250°C. MS data from 40-400 mass-to-charge ratio (*m*/*z*) were collected after a 13 min solvent

delay. Metabolite quantification (n=3) was based on normalization to the internal standard 1-eicosene (www.sigmaaldrich.com) and OD_{600} at time of induction of protein expression.

NMR analysis

For NMR analysis, ≥1 mg of diterpene products was enzymatically produced as outlined above and purified by silica chromatography and semi-preparative HPLC as previously described (Murphy et al., 2019). Purified compounds were dissolved in deuterated chloroform ($CDCl_3$; www.sigmaaldrich.com) containing 0.03% (v/v) tetramethylsilane (TMS). NMR 1D (^{1}H and ^{13}C) and 2D (HSQC, COSY, HMBC and NOESY) spectra were acquired on a Bruker Avance III 800 MHz spectrometer (www.bruker.com) equipped with a 5 mm CPTCI cryoprobe using Bruker TopSpin 3.2 software and analyzed with MestReNova 11.0.2 software (https://mestrelab.com/). Chemical shifts were calibrated against known chloroform (^{1}H 7.26 and ^{13}C 77.0 ppm) signals.

Homology modeling and molecular docking

Homology models CYP71Z25-29 were generated with RosettaCM (Song et al., 2013) using the crystal structure of *Salvia miltiorrhiza* CYP76AH1 (Gu et al., 2019) (PDB-ID: 5YM3) as a template, and the lowest energy models were selected for docking with RosettaDock (Meiler and Baker, 2006; Davis and Baker, 2009). Input native protein structures almost invariably have regions that score poorly with force fields due to energetic strain, and minimization protocols commonly lead to increased deviation from original wild-type structure representing stable proteins. To mitigate these limitations cycles of minimization with combined backbone/sidechain restraints that are Pareto-optimal with respect to RMSD to the native structure and energetic

strain reduction were used to relax the template protein structure (Nivón et al., 2013). The full-length sequences for all targets and templates were aligned using PROMALS3D (Pei and Grishin, 2014). Each target sequence was respectively threaded onto each template and threaded partial models aligned in a single global frame. Full-chain models were then generated by Monte Carlo sampling guided by the Rosetta low-resolution energy function supplemented with distance restraints from the template structures and a penalty for separation in space of residues adjacent in the sequence. Structures were built using a Rosetta ‘‘fold tree’’ (Das and Baker, 2008). The global position of each segment was represented in Cartesian space, whereas the residue backbone and side-chain conformation in each segment were represented in torsion space. Using the aligned target and template sequences, evolutionary constraints were calculated and used for modeling (Thompson and Baker, 2011). A total of 500 homology models were generated for each variant, where the model with the lowest overall protein score (“total score”) was utilized for docking each substrate. First, the heme co-factor was docked into the model, followed by docking of the substrate variations [i.e., three possible C15 and C16 substitution arrangements for all five tested substrates: hydroxy (C15=OH, C16=H), pyrophosphate (C15=OPP, C16=H) and dihydroxy (C15=OH, C16=OH)] into the heme-model complex. The reactive carbon was heavily weighted within Rosetta to be constrained to a distance of 2±1 Å. Each docking simulation generated 1,000 docked poses that were filtered by “high” constraint (CST) scores, subsequently by total score (Sc) for the lowest 25%, and by interaction energy (IE) for the remaining lowest 25%.

Site-directed mutagenesis

Select point mutants were generated using whole-plasmid PCR amplification with site-specific sense and anti-sense oligonucleotides (Table S3) and Phusion HF Master Mix polymerase (www.neb.com). *Dpn*1 treatment was applied to remove template plasmids before transformation into DH5α cells for plasmid propagation. All mutants were sequence verified and functionally characterized using *E. coli* co-expression assays as described above.

In vivo feeding study

For substrate feeding assays, the constructs pETDuet-1:*Zm*CPR2/CYP71Z25 and pETDuet-1:*Zm*CPR2/CYP71Z29 were individually expressed in *E. coli* as described above. Expression of the base plasmid pETDuet-1:*Zm*CPR2 was used as a control. At the time of IPTG induction of protein expression, 10 μM of the diterpene alcohol substrates, **15** or **16**, dissolved in 1:1 (v/v) DMSO:MeOH were added to the culture, followed by incubation and metabolite analysis as outlined above.

Metabolite profiling of tissue extracts

Frozen tissue (~500 mg) was ground to a fine powder and metabolites were extracted in hexane:ethyl acetate (Hex:EA; 80:20) with shaking overnight at 200 RPM at 12°C. Root extracts were air-dried, re-dissolved in Hex:EA, and concentrated to a volume of 1 mL for GC-MS analysis as outlined above. Leaf extracts were treated in the same manner with the addition of partially purifying extracts over a mock silica column as previously described prior to analysis by GC-MS (Muchlinski et al., 2019). Relative metabolite quantification (n=3) was based on normalization of the analytes to the internal standard (1-eicosene; www.sigmaaldrich.com) and gDW.

579

580 **Transcriptome profiling of drought-elicited switchgrass tissues**

581 Switchgrass plants (var. Alamo AP13) were propagated from tillers to maintain low genetic
582 variation. Plants were cultivated in 9.5 L pots in a randomized block design under greenhouse
583 conditions to reproductive stage R1, with a 16hr light/8hr dark photoperiod and ~22/17°C
584 day/night temperature prior to drought treatment. Drought stress treatment was applied by
585 withholding water for four weeks, compared to control plants receiving daily drip irrigation with
586 nutrient solution. Relative soil water content was measured weekly using a HydroSense II probe
587 (Campbell Scientific). Leaf and root tissue of droughted and control plants (n=6) were collected
588 weekly and flash-frozen in liquid nitrogen for later processing. Total RNA was extracted from
589 100 mg of tissue using a Monarch® Total RNA Miniprep Kit (www.neb.com) and treated with
590 *DNase I* for genomic DNA removal. Preparation of cDNA libraries and transcriptome
591 sequencing was performed by Novogene Co. Ltd. (https://en.novogene.com). In brief, following
592 RNA integrity analysis and quantitation, cDNA libraries were generated using a
593 NEBNext®Ultra™RNA Library Prep Kit (www.neb.com) and sequenced on an Illumina
594 Novaseq 6000 sequencing platform generating 40-80 million 150 bp paired-end reads per
595 sample. Raw reads were processed using FastQC
596 (www.bioinformatics.babraham.ac.uk/projects/fastqc/), and high-quality reads were aligned to
597 the reference genome (*P. virgatum* var. Alamo AP13 v5.1) using HISAT2. Heatmaps were
598 generated using the 'pheatmap' package in R (cran-project.org, version 3.6.3).

599

600 **Phylogenetic analysis**

601 A maximum likelihood phylogenetic tree was generated using the PhyML (http://www.atgc-
602 montpellier.fr/phyml/) server with four rate substitution categories, LG substitution model,
603 BIONJ starting tree and 500 bootstrap repetitions (Guindon et al., 2010).
604
605 **Accession numbers**
606 Nucleotide sequences of P450 genes and enzymes characterized in this study are available
607 on Phytozome (https://phytozome.jgi.doe.gov): *CYP71Z25* (*Pavir.1KG341400*), *CYP71Z26*
608 (*Pavir.1KG382300*), *CYP71Z27* (*Pavir.1KG382400*), *CYP71Z28* (*Pavir.1NG304500*),
609 *CYP71Z29* (*Pavir.1NG309700*). Gene identifiers based on *P. virgatum* (var. Alamo AP13)
610 genome (version v5.1). The RNA-seq data have been submitted to the Sequence Read Archive
611 (SRA), accession no. PRJNA644234.
612
613 **Acknowledgements**
614 We gratefully acknowledge the US Department of Energy Joint Genome Institute (DOE JGI) and
615 collaborators for prepublication access to the *Panicum virgatum* v1.1 and v4.1 genome sequence
616 data produced by DOE JGI. We further thank Dr. Reuben Peters (Iowa State University, USA)
617 for providing the pIRS and pGGxC constructs, the UC Davis Genome Center Bioinformatics
618 Core for providing high-performance computing resources, and Dr. Malay Saha (Nobel Research
619 Institute, USA) for providing tillers of *P. virgatum* var. Alamo AP13.
620
621 **Author Contributions**
622 P.Z. conceived the original research and oversaw data analysis; A.M. and M.J. performed most
623 experiments and data analyses; K.T. conducted plant drought stress experiments, metabolite

624 profiling of plant tissues, and transcriptome analysis; J.S.F. and J.S. performed protein modeling
625 and molecular docking studies; K.A.P. performed NMR structural analyses; L.C., D.D and Y.C.
626 assisted with site-directed mutagenesis studies; J.T.L. performed gene synteny studies; A.M.,
627 M.J. and P.Z. wrote the article with contributions from all authors. All authors have read and
628 approved the manuscript.
629

630 **Conflict of interest statement**

631 The authors declare that they have no conflict of interest in accordance with the journal policy.
632

633 **Funding**

634 Financial support for this work was provided by the U.S. Department of Energy (DOE) Early
635 Career Research Program (DE-SC0019178, to PZ), and a DOE Joint Genome Institute (JGI)
636 DNA Synthesis Science Program (grant #2568, to PZ). The gene synthesis work conducted by
637 the U.S. Department of Energy Joint Genome Institute (JGI), a DOE Office of Science User
638 Facility, is supported by the Office of Science of the U.S. Department of Energy under Contract
639 No. DE-AC02-05CH11231.
640

641 **Supplementary Information:**

642 **Fig. S1:** Identification of CYP71Z25-29 paralogs.

643 **Fig. S2:** Diterpenoid-metabolic pathways and compounds relevant to this study.

644 **Fig. S3:** Functional characterization of switchgrass CYP71Z25-29.

645 **Fig S4:** NMR analysis of *syn*-15,16-epoxy-8(17),13(16),14-triene (17).

646 **Fig S5:** NMR analysis of 15,16-epoxy-8,13(16),14-triene (18).

Parsed Citations

Bailey-Serres J, Parker JE, Ainsworth EA, Oldroyd GED, Schroeder JI (2019) Genetic strategies for improving crop yields. Nature 575: 109-118
Google Scholar: Author Only Title Only Author and Title

Banerjee A, Hamberger B (2018) P450s controlling metabolic bifurcations in plant terpene specialized metabolism. Phytochem Rev 17: 81-111
Google Scholar: Author Only Title Only Author and Title

Bao H, Zhang Q, Ye Y, Lin L (2016) Naturally occurring furanoditerpenoids: distribution, chemistry and their pharmacological activities. Phytochemistry Reviews 16: 235-270
Google Scholar: Author Only Title Only Author and Title

Bennetzen JL, Schmutz J, Wang H, Percifield R, Hawkins J, Pontaroli AC, Estep M, Feng L, Vaughn JN, Grimwood J, Jenkins J, Barry K, Lindquist E, Hellsten U, Deshpande S, Wang X, Wu X, Mitros T, Triplett J, Yang X, Ye CY, Mauro-Herrera M, Wang L, Li P, Sharma M, Sharma R, Ronald PC, Panaud O, Kellogg EA, Brutnell TP, Doust AN, Tuskan GA, Rokhsar D, Devos KM (2012) Reference genome sequence of the model plant Setaria. Nat Biotechnol 30: 555-561
Google Scholar: Author Only Title Only Author and Title

Bertea CM, Schalk M, Karp F, Maffei M, Croteau R (2001) Demonstration that menthofuran synthase of mint (Mentha) is a cytochrome P450 monooxygenase: Cloning, functional expression, and characterization of the responsible gene. Archives of Biochemistry and Biophysics 390: 279-286
Google Scholar: Author Only Title Only Author and Title

Bevan MW, Uauy C, Wulff BB, Zhou J, Krasileva K, Clark MD (2017) Genomic innovation for crop improvement. Nature 543: 346-354
Google Scholar: Author Only Title Only Author and Title

Christensen SA, Huffaker A, Sims J, Hunter CT, Block A, Vaughan MM, Willett D, Romero M, Mylroie JE, Williams WP, Schmelz EA (2018) Fungal and herbivore elicitation of the novel maize sesquiterpenoid, zealexin A4, is attenuated by elevated CO2. Planta 247: 863-873
Google Scholar: Author Only Title Only Author and Title

Das R, Baker D (2008) Macromolecular modeling with rosetta. Annu Rev Biochem 77: 363-382
Google Scholar: Author Only Title Only Author and Title

Davis IW, Baker D (2009) RosettaLigand docking with full ligand and receptor flexibility. J Mol Biol 385: 381-392
Google Scholar: Author Only Title Only Author and Title

Ding Y, Murphy KM, Poretsky E, Mafu S, Yang B, Char SN, Christensen SA, Saldivar E, Wu M, Wang Q, Ji L, Schmitz RJ, Kremling KA, Buckler ES, Shen Z, Briggs SP, Bohlmann J, Sher A, Castro-Falcon G, Hughes CC, Huffaker A, Zerbe P, Schmelz EA (2019) Multiple genes recruited from hormone pathways partition maize diterpenoid defences. Nat Plants 5: 1043-1056
Google Scholar: Author Only Title Only Author and Title

DOE-JGI Panicum hallii v2.0, DOE-JGI, http://phytozome.jgi.doe.gov.

DOE-JGI(b) Panicum hallii v3.1 (Hall's panicgrass) FIL2 var. filipes. In, http://phytozome.jgi.doe.gov/

Dueholm B, Krieger C, Drew D, Olry A, Kamo T, Taboureau O, Weitzel C, Bourgaud F, Hehn A, Simonsen HT (2015) Evolution of substrate recognition sites (SRSs) in cytochromes P450 from Apiaceae exemplified by the CYP71AJ subfamily. BMC Evol Biol 15: 122
Google Scholar: Author Only Title Only Author and Title

Gu M, Wang M, Guo J, Shi C, Deng J, Huang L, Chang Z (2019) Crystal structure of CYP76AH1 in 4-PI-bound state from Salvia miltiorrhiza. Biochem Biophys Res Commun 511: 813-819
Google Scholar: Author Only Title Only Author and Title

Guindon S, Dufayard JF, Lefort V, Anisimova M, Hordijk W, Gascuel O (2010) New algorithms and methods to estimate maximum-likelihood phylogenies: assessing the performance of PhyML 3.0. Syst. Biol. 59: 307-321
Google Scholar: Author Only Title Only Author and Title

Harris LJ, Saparno A, Johnston A, Prisic S, Xu M, Allard S, Kathiresan A, Ouellet T, Peters RJ (2005) The maize An2 gene is induced by Fusarium attack and encodes an ent-copalyl diphosphate synthase. Plant Mol Biol 59: 881-894
Google Scholar: Author Only Title Only Author and Title

Horie K, Inoue Y, Sakai M, Yao Q, Tanimoto Y, Koga J, Toshima H, Hasegawa M (2015) Identification of UV-Induced Diterpenes Including a New Diterpene Phytoalexin, Phytocassane F, from Rice Leaves by Complementary GC/MS and LC/MS Approaches. J Agric Food Chem 63: 4050-4059
Google Scholar: Author Only Title Only Author and Title

Jez JM, Lee SG, Sherp AM (2016) The next green movement: Plant biology for the environment and sustainability. Science 353: 1241-1244
Google Scholar: Author Only Title Only Author and Title

Karunanithi PS, Berrios DI, Wang S, Davis J, Shen T, Fiehn O, Maloof JN, Zerbe P (2020) The foxtail millet (Setaria italica) terpene

synthase gene family. Plant J
Google Scholar: Author Only Title Only Author and Title

Kivell BM, Ewald AW, Prisinzano TE (2014) Salvinorin A analogs and other kappa-opioid receptor compounds as treatments for cocaine abuse. Adv Pharmacol 69: 481-511
Google Scholar: Author Only Title Only Author and Title

Liu Y, Zhang X, Tran H, Shan L, Kim J, Childs K, Ervin EH, Frazier T, Zhao B (2015) Assessment of drought tolerance of 49 switchgrass (Panicum virgatum) genotypes using physiological and morphological parameters. Biotechnol Biofuels 8: 152
Google Scholar: Author Only Title Only Author and Title

Lovell JT, Jenkins J, Lowry DB, Mamidi S, Sreedasyam A, Weng X, Barry K, Bonnette J, Campitelli B, Daum C, Gordon SP, Gould BA, Khasanova A, Lipzen A, MacQueen A, Palacio-Mejía JD, Plott C, Shakirov EV, Shu S, Yoshinaga Y, Zane M, Kudrna D, Talag JD, Rokhsar D, Grimwood J, Schmutz J, Juenger TE (2018) The genomic landscape of molecular responses to natural drought stress in Panicum hallii. Nat Commun 9: 5213
Google Scholar: Author Only Title Only Author and Title

Lovell JT, MacQueen AH, Mamidi S, Bonnette J, Jenkins J, Napier JD, Sreedasyam A, Healey A, Session A, Shu S, Barry K, Bonos S, Boston L, Daum C, Deshpande S, Ewing A, Grabowski PP, Haque T, Harrison M, Jiang J, Kudrna D, Lipzen A, Pendergast TH, Plott C, Qi P, Saski CA, Shakirov EV, Sims D, Sharma M, Sharma R, Stewart A, Singan VR, Tang Y, Thibivillier S, Webber J, Weng X, Williams M, Wu GA, Yoshinaga Y, Zane M, Zhang L, Zhang J, Behrman KD, Boe AR, Fay PA, Fritschi FB, Jastrow JD, Lloyd-Reilley J, Martínez-Reyna JM, Matamala R, Mitchell RB, Rouquette FM, Ronald P, Saha M, Tobias CM, Udvardi M, Wing RA, Wu Y, Bartley LE, Casler M, Devos KM, Lowry DB, Rokhsar DS, Grimwood J, Juenger TE, Schmutz J (2021) Genomic mechanisms of climate adaptation in polyploid bioenergy switchgrass. Nature
Google Scholar: Author Only Title Only Author and Title

Mafu S, Ding Y, Murphy KM, Yaacoobi O, Addison JB, Wang Q, Shen Z, Briggs SP, Bohlmann J, Castro-Falcon G, Hughes CC, Betsiashvili M, Huffaker A, Schmelz EA, Zerbe P (2018) Discovery, biosynthesis and stress-related accumulation of dolabradiene-derived defenses in maize. Plant Physiol
Google Scholar: Author Only Title Only Author and Title

Mao H, Liu J, Ren F, Peters RJ, Wang Q (2016) Characterization of CYP71Z18 indicates a role in maize zealexin biosynthesis. Phytochemistry 121: 4-10
Google Scholar: Author Only Title Only Author and Title

Meiler J, Baker D (2006) ROSETTALIGAND: protein-small molecule docking with full side-chain flexibility. Proteins 65: 538-548
Google Scholar: Author Only Title Only Author and Title

Meyer E, Aspinwall MJ, Lowry DB, Palacio-Mejia JD, Logan TL, Fay PA, Juenger TE (2014) Integrating transcriptional, metabolomic, and physiological responses to drought stress and recovery in switchgrass (Panicum virgatum L.). BMC Genomics 15: 1-15
Google Scholar: Author Only Title Only Author and Title

Morrone D, Hillwig ML, Mead ME, Lowry L, Fulton DB, Peters RJ (2011) Evident and latent plasticity across the rice diterpene synthase family with potential implications for the evolution of diterpenoid metabolism in the cereals. Biochem J 435: 589-595
Google Scholar: Author Only Title Only Author and Title

Morrone D, Lowry L, Determan MK, Hershey DM, Xu M, Peters RJ (2010) Increasing diterpene yield with a modular metabolic engineering system in E. coli: comparison of MEV and MEP isoprenoid precursor pathway engineering. Appl Microbiol Biotechnol 85: 1893-1906
Google Scholar: Author Only Title Only Author and Title

Muchlinski A, Chen X, Lovell JT, Köllner TG, Pelot KA, Zerbe P, Ruggiero M, Callaway L, Laliberte S, Chen F, Tholl D (2019) Biosynthesis and Emission of Stress-Induced Volatile Terpenes in Roots and Leaves of Switchgrass (Front Plant Sci 10: 1144

Murphy KM, Chung S, Fogla S, Minsky HB, Zhu KY, Zerbe P (2019) A Customizable Approach for the Enzymatic Production and Purification of Diterpenoid Natural Products. J Vis Exp
Google Scholar: Author Only Title Only Author and Title

Murphy KM, Ma LT, Ding Y, Schmelz EA, Zerbe P (2018) Functional Characterization of Two Class II Diterpene Synthases Indicates Additional Specialized Diterpenoid Pathways in Maize (Zea mays). Front Plant Sci 9: 1542
Google Scholar: Author Only Title Only Author and Title

Murphy KM, Zerbe P (2020) Specialized diterpenoid metabolism in monocot crops: Biosynthesis and chemical diversity. Phytochemistry 172: 112289
Google Scholar: Author Only Title Only Author and Title

Nelson R, Wiesner-Hanks T, Wisser R, Balint-Kurti P (2018) Navigating complexity to breed disease-resistant crops. Nat Rev Genet 19: 21-33
Google Scholar: Author Only Title Only Author and Title

Nivón LG, Moretti R, Baker D (2013) A Pareto-optimal refinement method for protein design scaffolds. PLoS One 8: e59004
Google Scholar: Author Only Title Only Author and Title

Park HL, Lee SW, Jung KH, Hahn TR, Cho MH (2013) Transcriptomic analysis of UV-treated rice leaves reveals UV-induced phytoalexin biosynthetic pathways and their regulatory networks in rice. Phytochemistry 96: 57-71
Google Scholar: Author Only Title Only Author and Title

Pei J, Grishin NV (2014) PROMALS3D: multiple protein sequence alignment enhanced with evolutionary and three-dimensional structural information. Methods Mol Biol 1079: 263-271
Google Scholar: Author Only Title Only Author and Title

Pelot KA, Chen R, Hagelthorn DM, Young CA, Addison JB, Muchlinski A, Tholl D, Zerbe P (2018) Functional diversity of diterpene synthases in the biofuel crop switchgrass. Plant Physiol
Google Scholar: Author Only Title Only Author and Title

Pelot KA, Mitchell R, Kwon M, Hagelthorn DM, Wardman JF, Chiang A, Bohlmann J, Ro DK, Zerbe P (2016) Biosynthesis of the psychotropic plant diterpene salvinorin A: Discovery and characterization of the Salvia divinorum clerodienyl diphosphate synthase. Plant J
Google Scholar: Author Only Title Only Author and Title

Pelot KA, Mitchell R, Kwon M, Hagelthorn DM, Wardman JF, Chiang A, Bohlmann J, Ro DK, Zerbe P (2017) Biosynthesis of the psychotropic plant diterpene salvinorin A: Discovery and characterization of the Salvia divinorum clerodienyl diphosphate synthase. Plant J 89: 885-897
Google Scholar: Author Only Title Only Author and Title

Peters RJ (2010) Two rings in them all: the labdane-related diterpenoids. Nat Prod Rep 27: 1521-1530
Google Scholar: Author Only Title Only Author and Title

Savary S, Willocquet L, Pethybridge SJ, Esker P, McRoberts N, Nelson A (2019) The global burden of pathogens and pests on major food crops. Nature Ecology & Evolution 3: 430-+
Google Scholar: Author Only Title Only Author and Title

Schmelz EA, Huffaker A, Sims JW, Christensen SA, Lu X, Okada K, Peters RJ (2014) Biosynthesis, elicitation and roles of monocot terpenoid phytoalexins. Plant J 79: 659-678
Google Scholar: Author Only Title Only Author and Title

Schmer MR, Vogel KP, Mitchell RB, Perrin RK (2008) Net energy of cellulosic ethanol from switchgrass. Proc Natl Acad Sci U S A 105: 464-469
Google Scholar: Author Only Title Only Author and Title

Song Y, DiMaio F, Wang RY, Kim D, Miles C, Brunette T, Thompson J, Baker D (2013) High-resolution comparative modeling with RosettaCM. Structure 21: 1735-1742
Google Scholar: Author Only Title Only Author and Title

Swaminathan S, Morrone D, Wang Q, Fulton DB, Peters RJ (2009) CYP76M7 is an ent-cassadiene C11alpha-hydroxylase defining a second multifunctional diterpenoid biosynthetic gene cluster in rice. Plant Cell 21: 3315-3325
Google Scholar: Author Only Title Only Author and Title

Tholl D (2015) Biosynthesis and biological functions of terpenoids in plants. Adv Biochem Eng Biotechnol 148: 63-106
Google Scholar: Author Only Title Only Author and Title

Thompson J, Baker D (2011) Incorporation of evolutionary information into Rosetta comparative modeling. Proteins 79: 2380-2388
Google Scholar: Author Only Title Only Author and Title

Vaughan MM, Christensen S, Schmelz EA, Huffaker A, McAuslane HJ, Alborn HT, Romero M, Allen LH, Teal PE (2015) Accumulation of terpenoid phytoalexins in maize roots is associated with drought tolerance. Plant Cell Environ 38: 2195-2207
Google Scholar: Author Only Title Only Author and Title

Vaughan MM, Huffaker A, Schmelz EA, Dafoe NJ, Christensen S, Sims J, Martins VF, Swerbilow J, Romero M, Alborn HT, Allen LH, Teal PE (2014) Effects of elevated [CO2] on maize defence against mycotoxigenic Fusarium verticillioides. Plant Cell Environ 37: 2691-2706
Google Scholar: Author Only Title Only Author and Title

Wu Y, Hillwig ML, Wang Q, Peters RJ (2011) Parsing a multifunctional biosynthetic gene cluster from rice: Biochemical characterization of CYP71Z6 & 7. FEBS Lett 585: 3446-3451
Google Scholar: Author Only Title Only Author and Title

Wu Y, Zhou K, Toyomasu T, Sugawara C, Oku M, Abe S, Usui M, Mitsuhashi W, Chono M, Chandler PM, Peters RJ (2012) Functional characterization of wheat copalyl diphosphate synthases sheds light on the early evolution of labdane-related diterpenoid metabolism in the cereals. Phytochemistry 84: 40-46
Google Scholar: Author Only Title Only Author and Title

Xingxing Li ADJ, Robert L. Last Switchgrass metabolomics reveals striking genotypic and developmental differences in saponins. In, Vol doi: https://doi.org/10.1101/2020.06.01.127720
Google Scholar: Author Only Title Only Author and Title

Xu M, Hillwig ML, Prisic S, Coates RM, Peters RJ (2004) Functional identification of rice syn-copalyl diphosphate synthase and its role in initiating biosynthesis of diterpenoid phytoalexin/allelopathic natural products. Plant J 39: 309-318

Google Scholar: Author Only Title Only Author and Title

Xu M, Wilderman PR, Morrone D, Xu J, Roy A, Margis-Pinheiro M, Upadhyaya NM, Coates RM, Peters RJ (2007) Functional characterization of the rice kaurene synthase-like gene family. Phytochemistry 68: 312-326

Google Scholar: Author Only Title Only Author and Title

Zerbe P, Bohlmann J (2015) Plant diterpene synthases: exploring modularity and metabolic diversity for bioengineering. Trends Biotechnol 33: 419-428

Google Scholar: Author Only Title Only Author and Title

Zerbe P, Rodriguez SM, Mafu S, Chiang A, Sandhu HK, O'Neil-Johnson M, Starks CM, Bohlmann J (2015) Exploring diterpene metabolism in non-model species: transcriptome-enabled discovery and functional characterization of labda-7,13E-dienyl diphosphate synthase from Grindelia robusta. Plant J 83: 783-793

Google Scholar: Author Only Title Only Author and Title

Zhou K, Xu M, Tiernan M, Xie Q, Toyomasu T, Sugawara C, Oku M, Usui M, Mitsuhashi W, Chono M, Chandler PM, Peters RJ (2012) Functional characterization of wheat ent-kaurene(-like) synthases indicates continuing evolution of labdane-related diterpenoid metabolism in the cereals. Phytochemistry 84: 47-55

Google Scholar: Author Only Title Only Author and Title

Zi J, Mafu S, Peters RJ (2014) To gibberellins and beyond! Surveying the evolution of (di)terpenoid metabolism. Annu Rev Plant Biol 65: 259-286

Google Scholar: Author Only Title Only Author and Title